nature physics

LETTERS

https://doi.org/10.1038/s41567-018-0300-z

Charge trapping and super-Poissonian noise centres in a cuprate superconductor

K. M. Bastiaans[1,4], D. Cho[1,4], T. Benschop[1], I. Battisti[1], Y. Huang[2], M. S. Golden[2], Q. Dong[3], Y. Jin[3], J. Zaanen[1] and M. P. Allan[1*]

The electronic properties of cuprate high-temperature superconductors in their normal state are highly two-dimensional: transport along the crystal planes is perfectly metallic, but is insulating along the perpendicular 'c-axis' direction. The ratio of the in-plane to the perpendicular resistance can exceed 10^4 (refs [1–4]). This anisotropy was identified as one of the mysteries of the cuprates early on[5,6], and although widely different proposals exist for its microscopic origin[7–9], there is little empirical information on the microscopic scale. Here, we elucidate the properties of the insulating layers with a newly developed scanning noise spectroscopy technique that can spatially map the current and its time-resolved fluctuations. We discover atomic-scale noise centres that exhibit megahertz current fluctuations 40 times the expectation from Poissonian noise, more than what has been observed in mesoscopic systems[10]. Such behaviour can happen only in highly polarizable insulators and represents strong evidence for trapping of charge in the charge reservoir layers. Our measurements suggest a picture of metallic layers separated by polarizable insulators within a three-dimensional superconducting state.

The difference between metals and insulators is that in the former, additional charge equilibrates in femtoseconds, whereas the latter can be statically charged. The coupling to the lattice is a necessary condition for the trapping of charge in insulators on macroscopic timescales, since electrons by themselves have too great a quantum mechanical behaviour to localize. The trapped charge is stabilized by the formation of static, localized polarons involving a reconfiguration of the atomic lattice. Strongly polarizable insulators such as $SrTiO_3$ exemplify this process. Such trapping of charge on slow timescales has been conjectured as a cause of the anomalous, highly resistive *c*-axis transport in the cuprate high-temperature superconductors[7], although there are alternative proposals such as incoherent transport[11,12]. However, for these materials, band structure theory predicts metallic transport along the *c*-axis due to the small but finite *c*-axis bandwidth of the order of 0.1 eV (ref. [13]). Here, we present firm evidence that such charge trapping processes do occur in superconducting cuprates measuring atomically resolved current fluctuations.

Quite generally, fluctuations of a signal in time—the noise—can be a powerful diagnostic tool as they contain information not present in the mean value. It has historically allowed differentiation between signals carried by particles and waves or between black body radiation and the coherent radiation of a laser. More recently, noise spectroscopy has established itself as a standard method of investigating mesoscopic systems. This is usually done by looking at the noise spectral power, $S(w) = <\delta I(t)\ \delta I(t')>$, where δI is the deviation of the current operator from the mean, and the averaging $<>$ is both quantum mechanical and statistical. Examples where noise transport measurements led to novel insights include the study of fractional charge[14], the doubling of charge in Andreev processes[15], and the vanishing of noise in break junctions at the quantum conductance[16]. We have succeeded in bringing this technique to the atomic scale in the tunnelling regime, discovering an unanticipated phenomenon when we applied it to a cuprate high-temperature superconductor.

The flow of classical, uncorrelated charged particles between two leads is a purely Poissonian process. Its noise is independent of frequency (white) and proportional to the charge q and the flow I of the carriers, $S = 2q|I|$, as a direct consequence of the discreteness of the carriers[17]. We define the normalized noise $S_n = S/2e|I|$, similar to the Fano factor. Thus $S_n = 1$ represents Poissonian noise, where $S_n < 1$ and $S_n > 1$ refer to sub-Poissonian and super-Poissonian noise, respectively (Fig. 1a, b). For an uncorrelated electronic liquid, one expects $S_n = 1$; for an exotic, spatially inhomogeneous electronic liquid, this is a priori unclear. Importantly, to find $S_n > 1$, processes in the system are required on a frequency scale that fits into the slow (megahertz) frequency window of the noise measurements. Another property of special relevance to our data is that such noise events may be completely invisible in the mean value of the current.

Our aim is thus to measure the fluctuations in the cuprates on the atomic scale. Bringing noise measurement to the tunnelling regime comes with unique challenges which have prevented any atomic-resolution shot noise measurement thus far. The central obstacle lies in the high impedance of the tunnelling junction, which is typically 0.3 GΩ to 10 GΩ. Together with the capacitance between tip and sample and the cable capacitance, the junction acts as low-pass filter, allowing transmission of signals only in the kilohertz range where $1/f$ noise and mechanical resonances dominate. Possible solutions include bootstrapping of an amplifier[18] or building an impedance-matching circuit[19]. Matching a gigaohm junction leads to considerable losses in the circuit. This is simplified when using the scanning tunnelling microscope (STM) in point contact mode or in the low-megaohm range[19,20] or by using methods based on force microscopy[21]; however, this increases interactions between tip and sample, making it more difficult to extrapolate the sample properties. Our goal is to perform noise measurements when in the tunnelling regime, with transparencies $t \sim 10^{-6}$. To accomplish this task, we build a resonance circuit with all inductors from superconducting niobium, and include a custom-built, high-mobility amplifier directly into the circuit, following the principle of devices built for

[1]Leiden Institute of Physics, Leiden University, Leiden, the Netherlands. [2]Van der Waals–Zeeman Institute, Institute of Physics, University of Amsterdam, Amsterdam, the Netherlands. [3]Centre de Nanosciences et de Nanotechnologies, CNRS, Univ. Paris-Sud, Univ. Paris-Saclay, C2N – Marcoussis, Marcoussis, France. [4]These authors contributed equally: K. M. Bastiaans, D. Cho. *e-mail: allan@physics.leidenuniv.nl

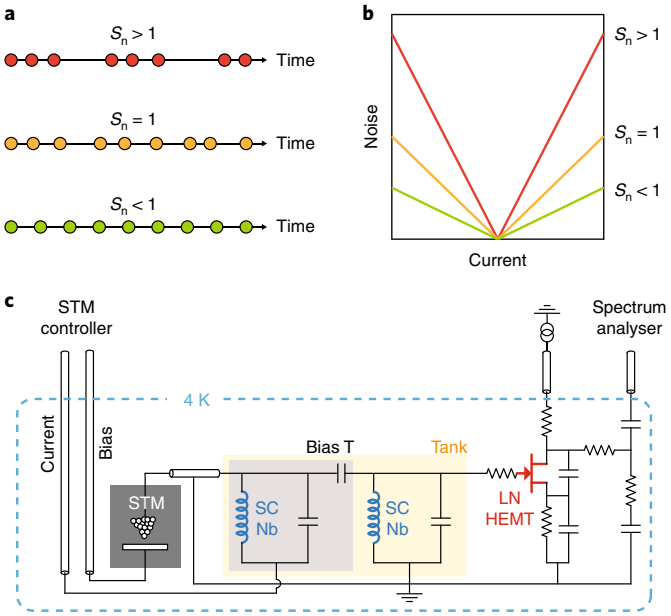

Fig. 1 | Scanning tunnelling noise spectroscopy as a new diagnostic tool. **a**, The classical flow of uncorrelated particles with charge q is a pure Poissonian process, $S = 2q|I|$. In the case of bunching, $S > 2q|I|$, and we refer to the noise as super-Poissonian (red). In the case of anti-bunching, $S < 2q|I|$, and we refer to the noise as sub-Poissonian (green). **b**, Noise S as a function of current in the cases described in **a**. **c**, Measurement circuit that allows for spatial mapping of the current fluctuations in the STM junction. A bias-T (indicated by the light grey area) separates the low- and high-frequency components of the signal. Superconducting niobium ($T_c = 9.2$ K; SC Nb, indicated in blue) inductors are used for the tank circuit (light orange box) that, in combination with the custom-built low-noise high electron mobility transistor (LN HEMT, in red), form the low-temperature amplification chain for noise measurements.

noise spectroscopy measurements in mesoscopic systems[22]. Figure 1c shows the amplification circuit that allows us to map out noise around 3 MHz with gigaohm junction resistances. We thoroughly tested our set-up on a gold sample (see Supplementary Information).

We first investigate with this new scanning noise microscopy instrument the cuprate high-temperature superconductors[23] with the hope of finding signs of the slow, glassy fluctuations associated with charge- or current loop order that have been claimed to show up in the noise[24–26]. These are not present, but instead we found a surprise that we will now explain.

As a sample material, we decided to use the slightly overdoped bi-layer cuprate $(Pb,Bi)_2Sr_2CaCu_2O_{8+\delta}$ with $T_c = 79$ K. The substitution of Pb for Bi has the advantage of supressing the characteristic super-modulation seen in many Bi-based cuprates, simplifying the interpretation and making higher-voltage measurements possible. We cleave the samples in ultrahigh vacuum at pressures below 10^{-10} mbar, and directly insert them into our STM head at 3.2 K. The single-crystal sample is held at a constant voltage V_{bias}, which drops over the approximately gigaohm junction between the tip and the uppermost CuO_2 layer (see Supplementary Information for details). The tunnelling process starts with electrons originating from the CuO_2 layer which then tunnel through the SrO and BiO layers[27]. Tunnelling through these charge reservoir layers does not have much effect on the STM signal, except for some spatial filtering[27,28]. Figure 2a shows a topographic image revealing atomic resolution. The square Bi-lattice is clearly resolved with some bright protrusions induced by Pb substitutions for Bi atoms (see Supplementary Information).

On recording the noise as a function of spatial location with atomic resolution at bias voltages of ± 0.1 eV we find homogeneously Poissonian noise (see Supplementary Information), with no sign of the fluctuating orders. However, this changes markedly when increasing the bias, as shown in Fig. 2b, c. Although most locations still exhibit Poissonian noise, a few atomic locations reveal striking enhancements of the noise. These super-Poissonian noise centres show noise values up to 40 times the expectation from Poissonian processes—more than anything that has been observed in mesoscopic systems[10]. We emphasize that the increase in noise is extremely localized, the width of the peaks in space being around 0.5 nm for most centres. The density of super-Poissonian noise centres is roughly 0.3%, referenced to the number of Cu atoms, and they are evenly distributed throughout the sample.

A key insight comes from the energy dependence of the noise. Noise spectra are shown in Fig. 2d–f. Below a certain threshold, the noise in the tunnelling current is purely Poissonian, $S_n = 1$. But above around 1 eV, or below around −650 meV, the normalized noise rises rapidly. Surprisingly, all noise centres appear to be highly asymmetric in energy: the noise enhancements at positive bias do not spatially correlate with the noise enhancement seen at negative energy. Although different locations show different strengths of noise enhancement, the onset energy seems to be independent of the noise centre, roughly −0.8 eV for the negative energy noise centres, and roughly +1 eV for the positive ones. This indicates a common mechanism and turns out to be an important diagnostic tool, as discussed below.

To understand these observations, it is worth taking a step back to look at engineered and natural systems that exhibit non-Poissonian noise, $S_n \neq 1$. In electronic systems this is most often sub-Poissonian noise[10,12,16,18], usually due to sequential tunnelling in quantum dots or Pauli exclusion effects. However, in the tunnelling regime considered here ($t \sim 10^{-6}$), the latter are minimal. Super-Poissonian noise on the other hand is a much rarer occurrence, as it always has to include some sort of interaction[10]. Experimentally, super-Poissonian noise was first observed in semiconductor double-wells and later in quantum dots[29]. Examples of super-Poissonian noise include bi-stable systems that lead to random telegraph noise in the transport, and coupling to inelastic modes[30]. Our data allow us to exclude all these mechanisms as the observed noise is bias dependent and asymmetric.

Instead, our data suggest the following scenario known from multi-level quantum dots. Two tunnelling processes are present, one fast, accounting for almost all the tunnelling current, and one slow, acting as a switch for the first process. This switching mechanism is usually based on Coulomb interaction. For example, if the state of the slow process is occupied, it raises the energy level of the state necessary for the fast process and effectively blocks it, as shown in Fig. 3. This leads to an effective switching, producing bunching of electrons that causes super-Poissonian noise. Such mechanisms have been discussed in detail for mesoscopic systems[10,12,31] and confirmed by experiments in multi-level quantum dots[32]. We note that this scenario predicts a clear threshold energy after which the noise increases, is asymmetric with respect to energy, and is localized on the atomic scale. The key insight that follows from our observations is that some slow process is involved, indicating a form of charge trapping that is known from strongly polarizable insulators, but not from a metal.

One expects these noise centres to correspond to some form of polarons being localized at defects in the crystal lattice, in contrast to more itinerant polarons at other locations. To shed light on their precise nature, we searched for impurity states, following earlier work[33] but now taking fully normalized $(dI/dV)/(I/V)$ density of states maps over a large energy range to be able to differentiate impurity states that overlap in energy. The energy-dependent $(dI/dV)/(I/V)$ maps reveal the spatial distribution of the different impurity states. Such states have been identified as apical oxygen vacancies, Sr(Ca)-site impurities, interstitial oxygen dopants and Pb

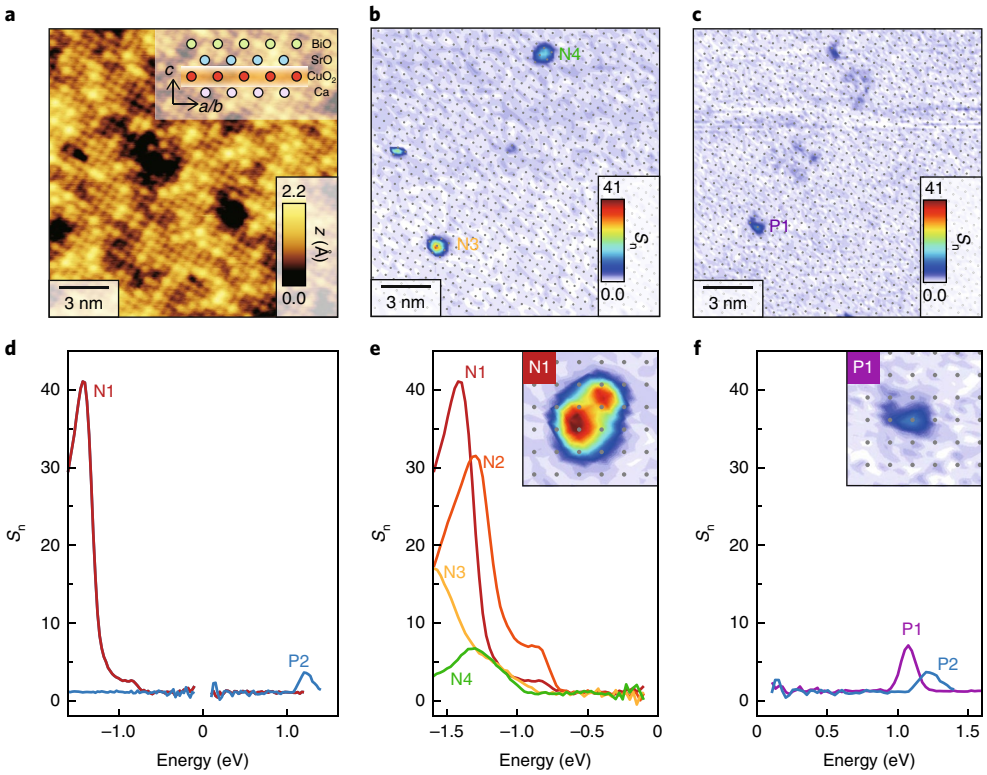

Fig. 2 | Observation of super-Poissonian noise centres. a, Atomic-resolution STM image of the BiO-terminated overdoped bi-layer cuprate $(Pb,Bi)_2Sr_2CaCu_2O_{8+\delta}$ surface in a 18.3 nm field of view (sample bias $V_{bias} = -0.10$ V, set-up current $I_S = 0.1$ nA). Pb substitutions for Bi are visible as bright protrusions. **b**,**c**, Spatially resolved, background-line-subtracted, noise maps at -1.2 eV (**b**) and +1.1 eV (**c**) in the same field of view as in **a**. The noise is normalized by the current simultaneously recorded at the same location. Most locations show homogeneous Poissonian noise ($S_n = 1$), but a few atomic locations reveal striking enhancements. N3, N4 and P1 indicate the negative and positive noise centres. Grey dots represent the Cu lattice sites. **d**, Representative noise spectra on the atomic locations that exhibit super-Poissonian noise show the strong asymmetry. **e**,**f**, Noise spectra on various negative (**e**) and positive (**f**) noise centres. Each inset shows the spatial distribution of the noise enhancements (see also Supplementary Information).

impurities. Figure 4 shows signatures of these specific states; details of which can be found in the Supplementary Information.

Most importantly, we find a clear correspondence between positive-energy noise centres and the +1.1 V impurity state, as shown in Fig. 4c, d. This impurity state has previously been identified as an apical oxygen vacancy[33] which, in the insulating oxygen materials, has various charge states stabilized by lattice distortions. This amounts to strong evidence for this signature being associated with the charge trapping process. The positive noise centres all show this signature of an impurity state in the charge reservoir layer through which tunnelling occurs but is modulated by a slow charge trapping process. Surprisingly, we do not observe a clear correspondence between a specific type of impurity resonance and the site of the negative noise centres. This might be because the state is dark due to filtering mechanisms[28], or because of stronger coupling to the CuO_2 layer.

In summary, we have presented direct evidence for the existence of slow charge trapping processes at defect sites in the form of the localized super-Poissonian noise signals. These are reminiscent of Coulombic impurities that occur generically in polarizable insulators, despite the three-dimensional superconducting state present in our samples. Although the atomic centres with noise enhancement are sparse, they demonstrate the polaronic nature of charge carriers tunnelling through the insulating layers. Apart from the noise centres, the polarons are probably itinerant to different degrees; a situation that at present cannot be described by theory. The *c*-axis physics of the cuprates thus appears to be in a literal sense similar to what is found in, for example, the Al–Al_2O_3–Al barriers employed for Josephson junctions: no coherent charge transport is possible for normal electrons, whereas the virtual tunnelling of Cooper pairs suffices for a coherent Josephson contact. In the cuprates, this is manifested in the form of the *c*-axis Josephson plasmons observed in the optical conductivity[34], emerging from a completely overdamped charge transport in the normal state[3]. The surprise is that apparently an oxidic layer that is only two atoms thick living in a metallic environment suffices for the polaronic trapping of charge.

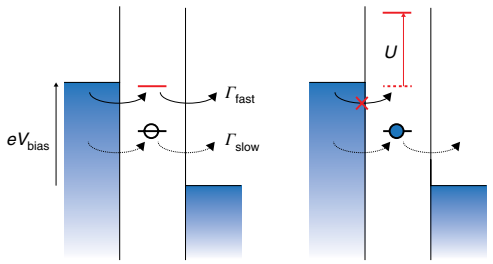

Fig. 3 | Example of modulated transport by slow charge trapping processes. Energy diagram of the co-tunnelling process via impurity states, indicated by red lines or black circles. The filled blue circle indicates an occupied state. Two tunnelling processes are possible; one of them has higher transmission rate (Γ_{fast}) than the other (Γ_{slow}) and dominates the total tunnelling current. Since they are strongly coupled by Coulomb energy (U), the tunnelling through the higher impurity level is prohibited by charge trapping of the lower one.

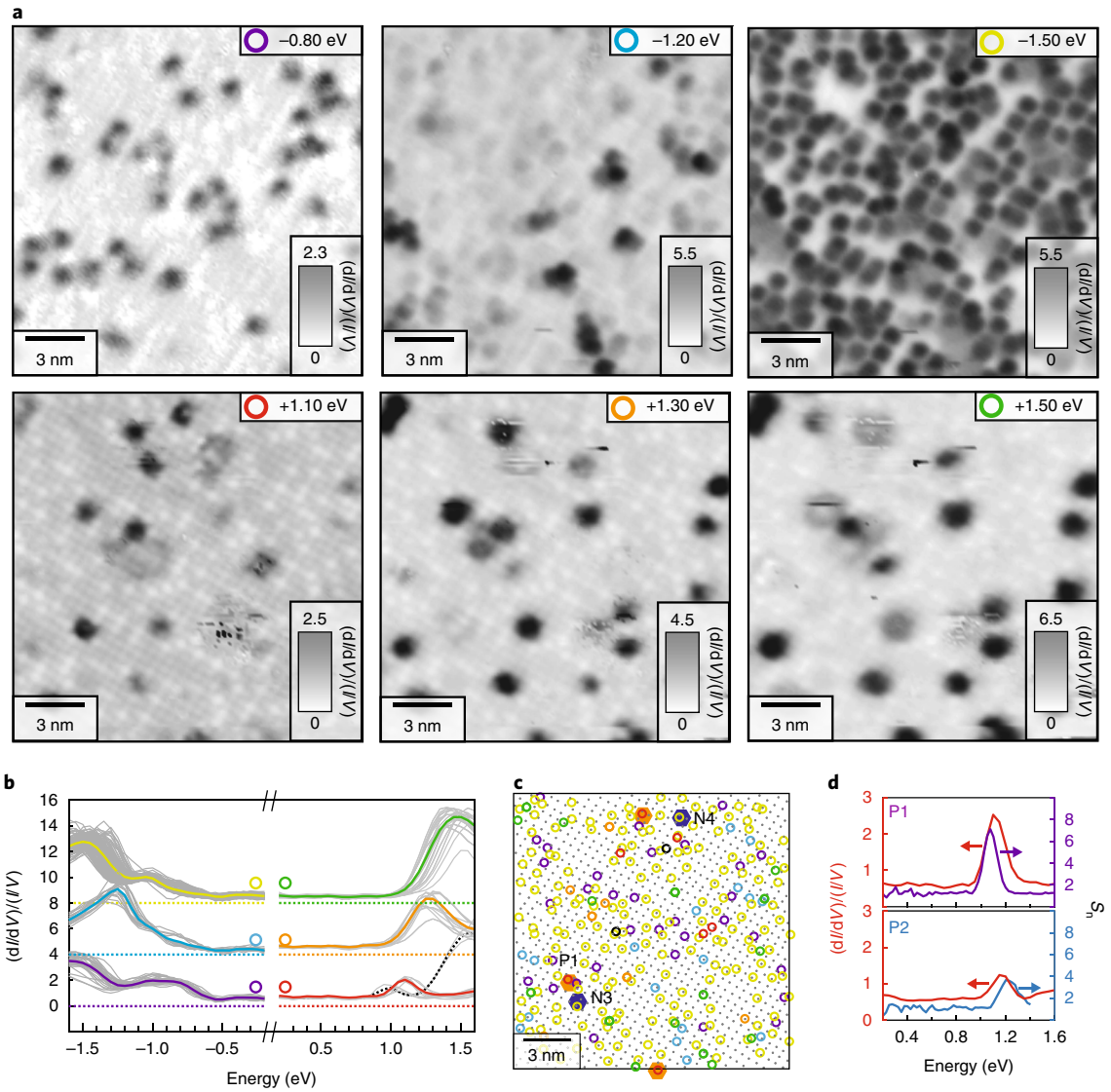

Fig. 4 | Bias-dependent conductance maps to identify impurity states and correlation with noise centres. a, Density of states at different energy levels: -1.5, -1.2, -0.8, +1.1, +1.3 and +1.5 eV. They were acquired in the same field of view as in Fig. 2a. The enhancement in normalized differential conductance ((d*I*/d*V*)/(*I*/*V*)) reveals the spatial distribution of various impurity states. **b**, Normalized differential conductance spectra taken on the different impurity states in **a**. The thick coloured lines represent the average of the individual grey spectra. **c**, Overview of all impurity states in this field of view. Grey dots represent the Cu-lattice. Various symbols corresponding to the different impurity states are classified based on **a**. The noise centres are indicated by the blue (negative) and red (positive) hexagons. **d**, Correspondence between positive-energy noise centres and the +1.1 V impurity state. P1 and P2 correspond to the positive noise centres shown in Fig. 2 and Supplementary Fig. 5.

The role of the '*c*-axis phenomena' in the mechanism of high-temperature superconductivity is a long-standing question[5,6,34], as is the unusual nature of the coupling of the polar insulator phonons to the electrons[5,6,8,9,35]. This acquired new impetus recently with the discovery that when a single layer of FeSe is removed from bulk and put on an polarizable insulator, the critical temperature increases by a factor of four[36], with evidence reported suggesting that the coupling to the polarizable insulating substrate may indeed play a critical role[37]. Further, interfaces of the polarizable insulators $SrTiO_3$ and $LaAlO_3$ host two-dimensional superconductors with the highest T_c per charge density ratio[35]. So much is clear from our findings, that even for the atomically thin insulating layers, the polar electron–phonon interactions are severe enough to slow down electronic motions to macroscopic timescales. Although a great challenge for established theory, this conundrum deserves further close consideration.

Online content

Any methods, additional references, Nature Research reporting summaries, source data, statements of data availability and associated accession codes are available at https://doi.org/10.1038/s41567-018-0300-z.

Received: 29 June 2018; Accepted: 3 September 2018;
Published online: 8 October 2018

References

1. Watanabe, T., Fujii, T. & Matsuda, A. Anisotropic resistivities of precisely oxygen controlled single-crystal $Bi_2Sr_2CaCu_2O_{8+\delta}$: Systematic study on 'spin gap' effect. *Phys. Rev. Lett.* **79**, 2113–2116 (1997).
2. Sordi, G., Sémon, P., Haule, K. & Tremblay, A. M. S. C-axis resistivity, pseudogap, superconductivity, and Widom line in doped Mott insulators. *Phys. Rev. B* **87**, 041101(R) (2013).

3. Levallois, J. et al. Temperature-dependent ellipsometry measurements of partial Coulomb energy in superconducting cuprates. *Phys. Rev. X* **6**, 031027 (2016).
4. Kim, J. H. et al. Strong damping of the *c*-axis plasmon in high-T_c cuprate superconductors. *Physica C* **247**, 297–308 (1995).
5. Anderson, P. W. Experimental constraints on the theory of high-T_c superconductivity. *Science* **256**, 1526–1531 (1992).
6. Leggett, A. J. A. 'midinfrared' scenario for cuprate superconductivity. *Proc. Natl Acad. Sci. USA* **96**, 8365–8372 (1999).
7. Gutman, D. B. & Maslov, D. L. Anomalous *c*-axis transport in layered metals. *Phys. Rev. Lett.* **99**, 196602 (2007).
8. Johnston, S. et al. Systematic study of electron–phonon coupling to oxygen modes across the cuprates. *Phys. Rev. B* **82**, 064513 (2010).
9. Meevasana, W., Devereaux, T. P., Nagaosa, N., Shen, Z. X. & Zaanen, J. Calculation of overdamped *c*-axis charge dynamics and the coupling to polar phonons in cuprate superconductors. *Phys. Rev. B* **74**, 174524 (2006).
10. Blanter, Y. M. in *CFN Lectures on Functional Nanostructures* Vol. 2 (eds Vojta, M., Röthig, C. & Schön, G.) Ch. 3 (Springer, Berlin, Heidelberg, 2010)
11. Anderson, P. W. & Zou, Z. 'Normal' tunneling and 'normal' transport: Diagnostics for the resonating-valence-bond state. *Phys. Rev. Lett.* **60**, 132–135 (1988).
12. Moses, P. & Mc Kenzie, R. H. Comparison of coherent and weakly incoherent transport models for the interlayer magnetoresistance of layered Fermi liquids. *Phys. Rev. B* **60**, 7998–8011 (1999).
13. Markiewicz, R. S., Sahrakorpi, S., Lindroos, M., Lin, H. & Bansil, A. One-band tight-binding model parametrization of the high-T_c cuprates including the effect of k_z dispersion. *Phys. Rev. B* **72**, 54519 (2005).
14. de-Picciotto, R. et al. Direct observation of a fractional charge. *Nature* **389**, 162–164 (1997).
15. Ronen, Y. et al. Charge of a quasiparticle in a superconductor. *Proc. Natl Acad. Sci. USA* **113**, 1743–1748 (2016).
16. van den Brom, H. & van Ruitenbeek, J. Quantum suppression of shot noise in atom-size metallic contacts. *Phys. Rev. Lett.* **82**, 1526–1529 (1999).
17. Blanter, Y. M. & Büttiker, M. Transition from sub-Poissonian to super-Poissonian shot noise in resonant quantum wells. *Phys. Rev. B* **59**, 10217–10226 (1999).
18. Birk, H., Jong, M., De & Schönenberger, C. Shot-noise suppression in the single-electron tunneling regime. *Phys. Rev. Lett.* **75**, 1610–1613 (1995).
19. Kemiktarak, U., Ndukum, T., Schwab, K. C. & Ekinci, K. L. Radio-frequency scanning tunnelling microscopy. *Nature* **450**, 85–88 (2007).
20. Burtzlaff, A., Schneider, N. L., Weismann, A. & Berndt, R. Shot noise from single atom contacts in a scanning tunneling microscope. *Surf. Sci.* **643**, 10–12 (2016).
21. Sung, M. G. et al. Scanning noise microscopy on graphene devices. *ACS Nano* **5**, 8620–8628 (2011).
22. DiCarlo, L. et al. System for measuring auto- and cross correlation of current noise at low temperatures. *Rev. Sci. Instrum.* **77**, 073906 (2006).
23. Keimer, B., Kivelson, S. A., Norman, M. R., Uchida, S. & Zaanen, J. From quantum matter to high-temperature superconductivity in copper oxides. *Nature* **518**, 179–186 (2015).
24. Carlson, E. W., Dahmen, K. A., Fradkin, E. & Kivelson, S. A. Hysteresis and noise from electronic nematicity in high-temperature superconductors. *Phys. Rev. Lett.* **96**, 097003 (2006).
25. Kivelson, S. A., Bindloss, I. P., Fradkin, E. & Oganesyan, V. How to detect fluctuating stripes in the high-temperature superconductors. *Rev. Mod. Phys.* **75**, 1201–1241 (2003).
26. Zhang, J. et al. Discovery of slow magnetic fluctuations and critical slowing down in the pseudogap phase of $YBa_2Cu_3O_y$. *Sci. Adv.* **4**, 5235 (2018).
27. Choubey, P., Kreisel, A., Berlijn, T., Andersen, B. M. & Hirschfeld, P. J. Universality of scanning tunneling microscopy in cuprate superconductors. *Phys. Rev. B* **96**, 174523 (2017).
28. Martin, I., Balatsky, A. V. & Zaanen, J. Impurity states and interlayer tunneling in high temperature superconductors. *Phys. Rev. Lett.* **88**, 097003 (2002).
29. Onac, E., Balestro, F., Trauzettel, B., Lodewijk, C. F. J. & Kouwenhoven, L. P. Shot-noise detection in a carbon nanotube quantum dot. *Phys. Rev. Lett.* **96**, 026803 (2006).
30. Thielmann, A., Hettler, M. H., Konig, J. & Schon, G. Cotunneling current and shot noise in quantum dots. *Phys. Rev. Lett.* **95**, 146806 (2005).
31. Safonov, S. S. et al. Enhanced shot noise in resonant tunneling via Interacting localized states. *Phys. Rev. Lett.* **91**, 136801 (2003).
32. Gustavsson, S. et al. Counting statistics and super-Poissonian noise in a quantum dot: Time-resolved measurements of electron transport. *Phys. Rev. B* **74**, 195305 (2006).
33. Zeljkovic, I. et al. Imaging the impact of single oxygen atoms on superconducting $Bi_{2+y}Sr_{2-y}CaCu2O_{8+x}$. *Science* **337**, 320–323 (2012).
34. Tsvetkov, A. A. et al. Global and local measures of the intrinsic Josephson coupling in $Tl_2Ba_2CuO_6$ as a test of the interlayer tunneling model. *Nature* **395**, 360–362 (1998).
35. Reyen, N. et al. Superconducting interface between insulating oxides. *Science* **317**, 1196–1199 (2007).
36. Wang, Q. Y. et al. Interface-induced high-temperature superconductivity in single unit-cell FeSe films on $SrTiO_3$. *Chin. Phys. Lett.* **29**, 037402 (2012).
37. Lee, J. J. et al. Interfacial mode coupling as the origin of the enhancement of T_c in FeSe films on $SrTiO_3$. *Nature* **515**, 245–248 (2014).

Acknowledgements

We thank C. Beenakker, A. Ben Hamida, Y. Blanter, D. Chatzopoulos, V. Cheianov, T. Klapwijk, M. Leeuwenhoek and J. van Ruitenbeek for help and valuable discussions. This project was financially supported by the European Research Council (ERC StG SpinMelt) and by the Netherlands Organisation for Scientific Research (NWO/OCW), as part of the Frontiers of Nanoscience programme, as well as through a Vidi grant (680-47-536).

Author contributions

K.M.B, D.C., T.B, I.B. and M.P.A. designed, developed and performed the noise-spectroscopy STM experiments and analysed the data, Y.H. and M.S.G. created the samples, Q.D. and J.Y. constructed the HEMT. M.P.A. supervised the study. All authors contributed to the interpretation of the data.

Competing interests

The authors declare no competing interests.

Additional information

Supplementary information is available for this paper at https://doi.org/10.1038/s41567-018-0300-z.

Reprints and permissions information is available at www.nature.com/reprints.

Correspondence and requests for materials should be addressed to M.P.A.

Publisher's note: Springer Nature remains neutral with regard to jurisdictional claims in published maps and institutional affiliations.

Methods

Single-crystal growth. The slightly overdoped bi-layer cuprate $(Pb,Bi)_2Sr_2CaCu_2O_{8+\delta}$ crystals were flux-grown in the standard manner with a Pb:Bi ratio of 0.4:1.6. Pb substitutions for Bi atoms show enhanced contrast in the atomic-resolution STM images[38,39]. The Pb content is highly consistent with the ratio. We characterized these sample by measuring the field-cooled magnetization superconducting transition using a DC superconducting quantum interference device (SQUID) magnetometer (MPMS XL from Quantum Design) in an applied field of 0.01 mT using the reciprocating sample option (RSO) (See Supplementary Information).

Scanning tunnelling microscopy and spectroscopy. The scanning tunnelling microscopy and spectroscopy measurements have been carried out with a modified commercial cryogenic STM (Unisoku USM 1500). The single crystals were cleaved in ultrahigh vacuum ($P < 5 \times 10^{-10}$ mbar) and directly transferred to the pre-cooled STM head ($T \sim 3.2$ K). We used mechanically sharpened Pt–Ir STM tips. The differential conductance (dI/dV) spectra were measured by a conventional lock-in technique with a voltage modulation of 50 mV and a frequency of 887 Hz. To minimize the set-up effect for LDOS maps, we normalized the dI/dV spectra with the total conductance (I/V).

Scanning noise spectroscopy. To overcome the limited bandwidth of conventional STM, we developed a low-temperature high-frequency amplifier including niobium superconducting coils and a custom-built low-noise high-mobility electron transistor[40,41]. The circuit is described in detail in the Supplementary Information and in ref. [4]. We used a Zurich Instruments MFLI digital spectrum analyser to measure the power spectral density of the noise. The integrated noise power as a function of current on the Au (111) surface and its slope are used to compute the normalized noise (S_n). If the charge transport is purely random, S_n is equal to 1, with deviations from 1 indicating the temporal correlation between charge carriers.

Data availability

The data that support the plots within this paper and other findings of this study are available from the corresponding author upon reasonable request.

References

38. Kinoda, G. et al. Direct determination of localized impurity levels located in the blocking layers of $Bi_2Sr_2CaCu_2O_y$ using scanning tunneling microscopy/spectroscopy. *Phys. Rev. B* **71**, 020502(R) (2005).
39. Fei, Y. et al. Electronic effect of doped oxygen atoms in Bi2201 superconductors determined by scanning tunneling microscopy. Preprint at https://arXiv.org/abs/1803.03400 (2018).
40. Dong, Q. et al. Ultra-low noise high electron mobility transistors for high-impedance and low-frequency deep cryogenic readout electronics. *Appl. Phys. Lett.* **105**, 013504 (2014).
41. Bastiaans, K. M. et al. Amplifier for scanning tunneling microscopy at MHz frequencies. Preprint at https://arXiv.org/abs/1806.00374 (2018).